

# Efforts Towards a Validated Time-Domain Model of an Oscillating Water Column with Control Components

Thomas Kelly\*, Thomas Dooley†, John Campbell‡ and John Ringwood\*

\*Department of Electronic Engineering  
Maynooth University, Co. Kildare, Ireland  
E-mail: thomas.e.kelly.2012@mumail.ie  
E-mail: john.ringwood@eeng.nuim.ie

†Centre for Renewable Energy at Dundalk IT  
Dundalk Institute of Technology, Dublin Rd., Dundalk, Ireland  
E-mail: thomas.dooley@dkit.ie

‡Wave Energy Ireland Ltd., Unit F1 Nutgrove Office Park, Rathfarnham, Dublin 14, Ireland  
E-mail: info@waveenergyireland.ie

**Abstract**—As part of the development process of a proposed offshore floating wind/wave platform, a scale-model testing programme has been carried out at a narrow tank facility on a single oscillating water column (OWC) device. Previous proof-of-concept testing was performed on a scale model of the proposed platform comprising thirty-two OWCs with control components. That testing programme, implemented at the Hydraulic and Maritime Research Centre, demonstrated the feasibility of the concept. However, the large number of interacting components in this complex system results in difficulties when attempting to study and model numerically the hydrodynamic and thermodynamic processes at work within the OWCs during operation. In order to better study these processes, the subsequent phase of narrow tank testing was planned based on a single-chamber OWC model as described herein. This model was constructed with similar dimensions and cross-sectional profile to that of one OWC chamber in the larger model. Various control components can be added to and removed from the new model to investigate in a systematic fashion the effect of each component. Theory to numerically model the OWC in various configurations has been developed. A comparison between the tank test results and those obtained for a specific setup is presented.

**Index Terms**—tank testing, numerical modelling, oscillating water column, control valves, plenum.

## I. INTRODUCTION

Of the numerous wave energy conversion technologies currently under investigation worldwide, perhaps the most established is that of the oscillating water column (OWC). A number of developers have considered the benefit of combining wave energy conversion with offshore wind energy conversion. One developer currently working on a combined offshore wind/wave energy conversion plant is Wave Energy Ireland Ltd. (WEI). The concept being developed envisages a floating, V-shaped platform comprising multiple oscillating water columns (MOWC) manifolded with airflow rectification for use with a unidirectional turbine. One or more offshore wind turbines would be installed on this platform. Proof-of-concept testing on the wave energy conversion elements of

this platform was performed on a stainless steel, 1:50 scale model in the ocean basin facility at the Hydraulic and Maritime Research Centre (HMRC) located in Co. Cork, Ireland. During this testing, air admittance valves were used to rectify the air flow, and venturis were used to simulate power take-off damping, as described in [1] and [2]. The primary focus of the testing at the HMRC was on the energy captured by the device in various configurations when subject to regular waves. Some work on characterising the hydrodynamic and thermodynamic behaviour of the device was performed, but the large number of interacting components resulted in difficulty in studying the behaviour of individual processes in the system. To further investigate these processes, and also characterise the individual components and provide data for the validation of numerical models, a single-chamber, fixed OWC model of similar dimensions to one chamber of the MOWC model was constructed in marine plywood for test in a narrow tank facility located at the Dundalk Institute of Technology (DkIT). As noted by [3], there is a lack of available experimental data for the validation of numerical models of OWCs. The work outlined in [3], which has parallels with the work described herein, details efforts towards a floating, MOWC using self-rectifying turbines. The main difference to the work in [3], is the inclusion here of control components and additional air volumes which can be introduced to the single-chamber OWC model to investigate the effect of, and characterise, each component in turn. This paper discusses the design and construction of this model and the various configurations in which the model was tested. Theory used for the generation of a numerical model is presented, and some results from the numerical model are compared to those obtained from the narrow tank testing. Further, a methodology for the derivation and verification of the frequency dependent added mass coefficients for an OWC based on results obtained from a commercial hydrodynamic solver is presented.

## II. SCALE MODEL

The single-chamber OWC model was made primarily from slices of marine plywood and spans the width of the DkIT narrow tank. The model represents a single chamber of the proposed MOWC device at a scale of 1:50. The geometry of the wetted surface of this model is similar in form to that of the wetted surface of the individual chambers described in [1]. Figure 1 is an exploded diagram illustrating the assembly of the model. The chamber comprises a rounded front lip (1), a curved back wall (2), two side walls (3) and (4) and top pieces (5), (6) and (7). To investigate the effect of control components used during the tests described in [1], the model may be reconfigured as described in Section IV below. Two 42-mm holes are cut in (5) which snugly receive a standard Wavin pipe of external diameter 42.75 mm. One of these holes is used to instal an adjustable orifice in the form of an iris valve onto the model, which may be used to introduce varying amounts of quadratic damping to the water column (see Phase 2 of the testing programme). These holes also allow air admittance valves (8), which allow air to flow in one direction only, to be installed on the model during some phases of the testing. Around these holes, rectangular tracks are routed in (5). The tracks allow for the installation of additional air volumes or plenums (9) as required in certain test phases. Finally, two plenums may be connected using standard Wavin fittings with the iris valve (10) located between them.

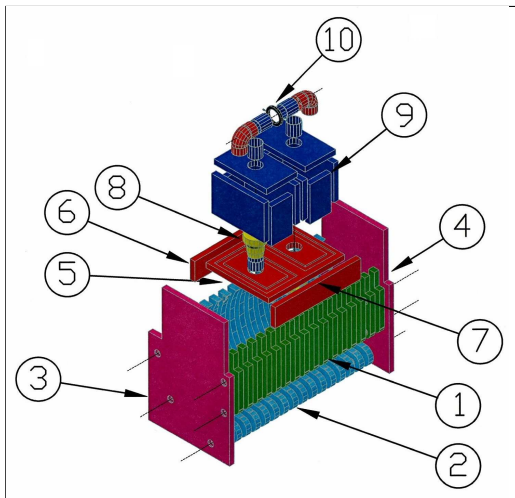


Fig. 1: Exploded single-chamber OWC model diagram.

## III. TEST FACILITY

The testing programme was conducted in a narrow tank facility located at DkIT. The tank is 18 m long, 350 mm wide and is filled to a depth of 1 m. The wavemaker comprises a hinged, wedge-shaped flap driven by a servo-motor. The setup incorporates a force feedback control system to reduce the effect of reflected waves. An absorbing parabolic beach is located at the opposite end of the tank from the wavemaker. The tank was calibrated during the summer of 2014. During this calibration process, all wave frequencies and amplitudes

used in the testing described herein were set with no model installed using the same water depth as present during the test described in Section IV. Reflections from the tank wall were also measured and found to be within acceptable limits.

A range of sensors were fitted to the tank and the OWC model. In order to record the free surface elevation within the tank, resistive wave probes were used. Two such probes were located at the transverse centre of the tank between the wavemaker and the model to monitor the generated wave height and frequency during the testing. A third wave probe measured the free surface elevation behind the model. The motions of the water column within the model were monitored by a fourth wave probe located at the centre of the water column at still water level conditions. Air pressure within the various air chambers (described in Section II above) were measured using 176PC14HD2 differential pressure transducers. Data was acquired and recorded using a USB-based CompactDAQ system supplied by National Instruments Corp. Figure 2 illustrates a schematic of the test facility and the model.

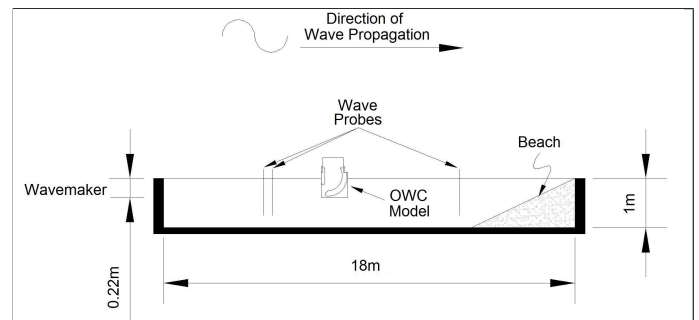


Fig. 2: Schematic of test facility with model.

## IV. TESTING PROGRAMME

There were six distinct phases to the DkIT narrow tanking programme.

*Phase 1:* This phase served to characterise the exciting force acting on the water column. The air chamber above the water column was first sealed, and the model was fixed in the tank with the lip submerged to a depth of 77.5 mm. The model was then subjected to regular waves of amplitudes ranging from 5 mm to 30 mm, in increments of 5 mm, for frequencies ranging from 0.4 Hz to 1.4 Hz, in increments of 0.1 Hz. These wave conditions were chosen to represent the typical range of waves found in the North Atlantic at a scale of 1:50, and are equivalent to wave periods of 5 s to approximately 17.7 s and wave heights of 0.5 m to 3 m at full scale. During this testing, the differential air pressure within the chamber of air above the water column, and the motion of the water column, were recorded. As air is effectively incompressible at this scale, the motion of the water column is negligible, as confirmed during this phase. Hence, the water column is effectively held fixed during this phase. Assuming the pressure of the air contained within the sealed chamber is uniform throughout, the force acting on the water column

can be found by multiplying the gauge pressure within the chamber by the surface area of the water column itself at any instant in time. This phase is modelled numerically using Equations 1 and 2 with  $\dot{m}_i = 0$ , (see Section V).

*Phase 2:* The purpose of this phase was to characterise the orifice (by determining the coefficient of discharge) and investigate non-linear effects within the system. An adjustable orifice was fitted to the base model using one of the 42-mm holes in ⑤ to allow air flow between the air chamber above the water column and atmosphere. The second 42-mm hole was sealed. The damping applied to the water column through the adjustable orifice was varied by changing the opening diameter of the orifice from 5 mm to 30 mm in steps of 5 mm. The model was subjected to the same incident waves of varying amplitudes and frequencies as in Phase 1 for each orifice diameter. As in Phase 1, the motions of the water column and the gauge pressure within the chamber were recorded. For Phases 1 and 2, data was sampled at 32 Hz. Phase 2 is modelled numerically using Equations 1, 2 and 3.

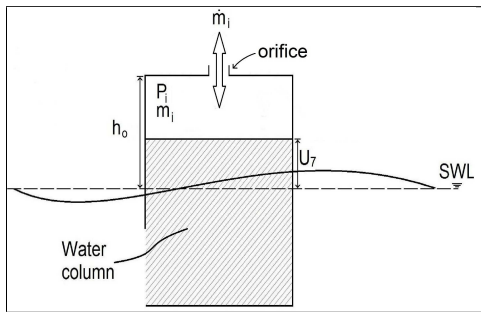


Fig. 3: Schematic of the OWC with an orifice (Phase 2).

*Phase 3:* This phase was designed to characterise the air admittance valves. The variable orifice was removed and two air admittance valves were installed on the model. If the air pressure within the OWC was greater than atmospheric pressure, air could flow through one valve from the OWC chamber to atmosphere: this valve is termed the exhalation valve. Should the air pressure within the OWC be less than atmospheric pressure, air could flow from atmosphere through the second valve into the OWC chamber: this valve is termed the inhalation valve. It was found that for wave amplitudes below 15 mm, the air pressure within the chamber did not increase or decrease sufficiently to overcome the valve inertia and stickage of either valve. As a result, data was only recorded for wave amplitudes varying from 15 mm to 30 mm, in increments of 5 mm, for the same range of wave frequencies as before. It was found that the minimum wave amplitude required to generate sufficient pressure to overcome valve inertia and stickage varied: the ambient temperature and time since the valve last opened appear to be two of the factors that influence this effect. As before, the water column motion and the differential pressure within the air chamber were recorded. It was found during this phase that

the pressure within the OWC chamber spiked as it overcame the stickage in the valve. To fully capture this effect, the sampling rate was increased to 1 kHz, and this rate was used for the remaining phases of testing. Phase 3 is modelled numerically using Equations 1, 2 and 4.

*Phase 4:* Phase 4 was intended to investigate the effect of a single plenum installed so that air flowing from the OWC chamber through the exhalation valve would discharge into this plenum before discharging to atmosphere. The aim was replicate the effect of one of the plenums which were used in [1] to manifold airflow from multiple chambers as part of the airflow rectification process and to smooth power delivery to the power take-off. The variable orifice used in Phase 1 was installed in the opening of the plenum. As before, various wave frequencies, amplitudes and orifice opening-diameters were tested. In addition to recording the motion of the water column and the differential pressure within the chamber, the differential air pressure in the plenum was also recorded during this phase. The motion of the water column during Phase 4 is modelled numerically using Equations 1 and 6 as described in Section V. The pressure within the chamber is modelled using Equation 2. The pressure within the plenum is modelled using Equation 5 and the mass flow equations are described in Table I.

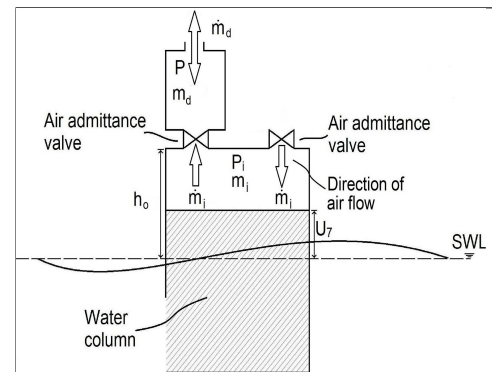


Fig. 4: Schematic of an OWC with air admittance valves and a single plenum (Phase 4).

*Phase 5:* Phase 5 was intended to investigate the effect of installing a second plenum so that air flowing through the inhalation valve into the OWC chamber would be drawn from this second plenum. The variable orifice was removed from the setup so that both plenums were in communication with atmosphere through a single, identical 42-mm hole in the lid of each plenum. In addition to the values recorded in Phase 4, the differential pressure in the second plenum was also recorded during this phase. The motion of the water column during Phase 5 is modelled numerically using Equations 6 and 8 as appropriate. The pressure within the chamber is modelled using Equation 2. The pressures within the plenums are modelled using Equations 5 and 7, and the mass flow equations are described in Table II.

## V. THEORY

The governing systems of coupled ordinary differential equations (ODEs) used to represent numerically the model are derived in [4]. The equations for each phase of testing are outlined below. They are derived by considering the mass flow rates and pressure changes throughout the system, as well as the motion of the water column. The process by which the mass flows are treated is similar to that described in [5].

In Phase 1, where no mass flow takes place, the motion of the water column is described by the modified Cummins Equation [6] presented in Equation 1. For this phase, and all subsequent phases, it is assumed that the water column acts in a pumping mode only, which is denoted by the subscript 7. Air pressures are denoted by  $P$ , and the subscript  $i$  denotes a property relating to the air chamber above the water column.

$$F_e = (m_7 + a_\infty) \ddot{U}_7 + \int_0^\infty k_7(t-\tau) \dot{U}_7(\tau) dt + c_{77} \dot{U}_7 + (P_i - P_{atmos}) \times A_{owc} \quad (1)$$

In Equation 1 above,  $F_e$  is the exciting force due to the incident wave,  $m_7$  is the mass of the water column,  $a_\infty$  is the infinite frequency added mass of the water column and  $U_7$  is the vertical displacement of the water column from the ‘at rest’ position.  $P_{atmos}$  is atmospheric air pressure,  $c_{77}$  is the hydrostatic stiffness of the water column, while the convolution term  $\int_0^\infty k_7(t-\tau) \dot{U}_7(\tau) dt$  represents the radiation forces, or the so-called ‘memory effect’ of the water column motions. The kernel of the convolution is represented by  $k_7$ , that is the impulse response function of the water column in the pumping mode.  $A_{owc}$  is the cross-sectional area of the water column. As the hydrodynamic parameters of the water column are modelled using linear, potential codes, non-linear forces, which are mainly due to viscous damping and vortex formation, are neglected in the following analysis. Furthermore, for the wave conditions used, non-linear hydrodynamic effects are minimal. The gauge pressure in the chamber, under the assumption of adiabatic conditions, is given by:

$$\Delta P = \frac{c_s^2}{V_i} \dot{m}_i - \gamma \frac{P_i}{V_i} \dot{V}_i \quad (2)$$

where  $c_s$  is the speed of sound in air,  $V_i$  is the volume of air above the water column within the OWC and  $\gamma$  is the heat capacity ratio of air. In the above equation,  $\Delta P = P_i - P_{atmos}$ . This equation applies to all phases and has been derived from consideration of the first law of thermodynamics. The same result was obtained in [7] for a reciprocating compressor. For Phase 1, the first term on the right-hand side of Equation 2 is zero as the mass of air in the OWC chamber,  $m_i$ , is constant: the flow of mass into or out of the chamber,  $\dot{m}_i$ , is zero. In Phase 1, the motion of the water column is due to the compression of air within the OWC chamber.

In Phase 2 of the testing, the OWC is in communication with atmosphere through an orifice. In this figure,  $h_o$  denotes the original height of the air chamber. The motion of the water column may be described by Equation 1 as before. Mass flow of air into the chamber is considered positive, and mass

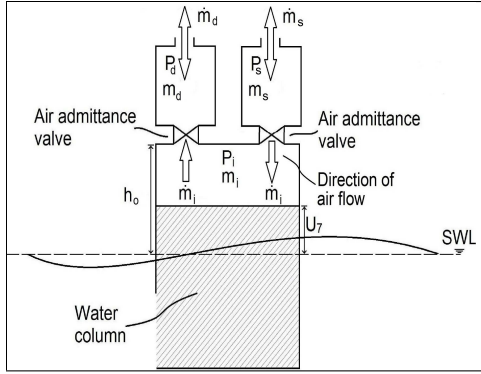


Fig. 5: Schematic of one OWC chamber with plenums installed on the inhalation and exhalation valves (Phase 5).

*Phase 6:* The purpose of the final phase of testing was to examine the effect of air compression within the system. In this phase, both plenums were connected via Wavin fittings with the variable orifice installed between them. This setup most closely resembled that of the stainless steel MOWC model tested in the HMRC. However, the air flow between plenums in the testing on the MOWC model depends on the phase difference between the motions of the water columns in that system. In contrast, in the single OWC narrow tank testing, any air flow between plenums which occurs can only arise due to air compressibility, and will thus be minimal. The differential pressure within the OWC chamber would thus be expected not to differ significantly from that in Phase 1. The same parameters were recorded during this phase as in Phase 5. The motion of the water column during Phase 5 is modelled numerically using Equations 6 and 8 as appropriate. The pressure within the chamber is modelled using Equation 2. The pressures within the plenums are modelled using Equations 5 and 7, and the mass flow equations are described in Table III.

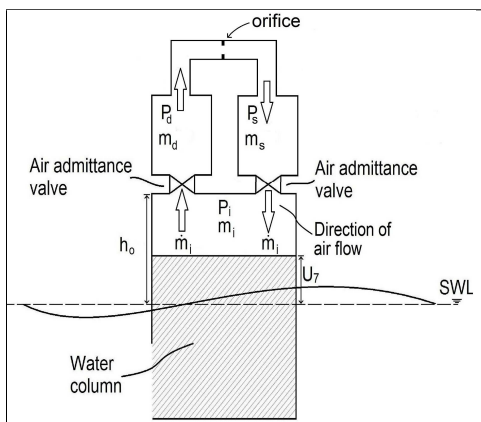


Fig. 6: Schematic of one OWC chamber, the high- and low-pressure plenum and conduit including orifice (Phase 6).

flow out of the chamber is considered negative. Under the assumption of incompressible flow, orifice theory [8] gives the mass flow rate into or out of the chamber as:

$$\dot{m}_i = Cd_o A_o \sqrt{2\rho_{air} |\Delta P|} \times sign \Delta P \quad (3)$$

where  $Cd_o$  is the coefficient of discharge of the orifice and  $A_o$  is the cross-sectional area of the orifice. The variation in chamber pressure is given by Equation 2. The volume of air in the chamber is proportional to the displacement of the water column, and the rate of change of that volume is proportional to the velocity of the water column. The above equations are implemented to simulate numerically the OWC model to generate the results presented in Section VII.

In Phase 3 the adjustable orifice was removed and two air admittance valves were installed. A difference in pressure across a valve causes a rubber diaphragm to lift and allows airflow through the valve in one direction only. Equations 1 and 2 still apply. However, the mass flow rate through a valve is given as [9]:

$$\dot{m}_i = Cd_v L_g h_{max} \sqrt{2\rho_{air} |\Delta P|} \times sign \Delta P \quad (4)$$

where  $Cd_v$  is the coefficient of discharge of the orifice,  $L_g$  is the distance between the rubber ring and the inside wall of the valve and  $h_{max}$  is the height the rubber ring lifts. It is assumed that the valves open and close instantaneously in response to a pressure difference. The forms of Equations 3 and 4 are identical, i.e., a constant is multiplied by the same function of a pressure difference. In Equation 3, this constant is given by  $Cd_o A_o$ , and in Equation 4, this constant is given by  $Cd_v L_g h_{max}$ , assuming the two air admittance valves are identical.

During Phase 4 an air plenum was installed on the model so that the exhalation valve is in communication with the plenum, and the plenum is in communication with atmosphere through an orifice. In addition to the three equations required to model Phase 2 numerically, a further two equations are needed to model the system setup used in Phase 4 in order to describe the rate of change of pressure, and the rate of change of mass, within the plenum. As derived in [2], the rate of change of pressure within the plenum,  $\dot{P}_d$ , with respect to the speed of sound,  $c_s$ , the mass flow rate into or out of the plenum,  $\dot{m}_d$ , and the volume of the plenum,  $V_d$ , is given by:

$$\dot{P}_d = \frac{c_s^2}{V_d} \dot{m}_d \quad (5)$$

The equations describing the mass flow rates and the motion of the water column at any instant depend on the state of the system. The term  $(P_i - P_{atmos}) \times A_{owc}$  in Equation 1 reflects the force acting on the water column due to the relative change of air pressure in the chamber with respect to atmosphere. In Phase 4 this force depends on the state of the air admittance valves. If the inhalation valve is open and the exhalation valve is closed, Equation 1 applies. If the exhalation valve is open

and the inhalation valve is closed, Equation 1 is modified to:

$$F_e = (m_7 + a_\infty) \ddot{U}_7 + \int_0^\infty k_7(t - \tau) \dot{U}_7(\tau) dt + c_{77} U_7 + (P_d - P_{atmos}) \times A_{owc} \quad (6)$$

Further, the rates of change of the masses of air in the chamber and in the plenum are governed by different equations depending on the current state of the valves. These mass flow equations are presented in Table I. The subscript  $o$  refers to a property of the orifice between the air plenum and atmosphere, and the subscript  $v$  refers to a property of an air admittance valve. The sign of the pressure difference is omitted but implied as shown in Equation 3.

TABLE I: Mass flow equations - Phase 4

Case	Mass flows
$P_i > P_d$ & $P_i > P_{atmos}$	$\dot{m}_i = -Cd_v L_g h_{max} \sqrt{2\rho_{air} (P_i - P_d)}$ $\dot{m}_d = Cd_v L_g h_{max} \sqrt{2\rho_{air} (P_i - P_d)}$ $-Cd_o A_o \sqrt{2\rho_{air} (P_d - P_{atmos})}$
$P_i < P_d$ & $P_i > P_{atmos}$	$\dot{m}_i = 0$ $\dot{m}_d = -Cd_o A_o \sqrt{2\rho_{air} (P_d - P_{atmos})}$
$P_i < P_d$ & $P_i < P_{atmos}$	$\dot{m}_i = Cd_v L_g h_{max} \sqrt{2\rho_{air} (P_{atmos} - P_i)}$ $\dot{m}_d = -Cd_o A_o \sqrt{2\rho_{air} (P_d - P_{atmos})}$

The setup in Phase 5 of the testing requires the introduction of a further variable,  $P_s$ , which is the pressure within the plenum from which the inhalation valve draws air. The mass flow rate into or out of this plenum is termed  $\dot{m}_s$ . Table II presents the mass flow rate equations depending on the valve conditions. The variation in pressure within the plenum on the inhalation

TABLE II: Mass flow equations - Phase 5

Case	Mass flows
$P_i > P_d$ & $P_i > P_{atmos}$	$\dot{m}_i = -Cd_v L_g h_{max} \sqrt{2\rho_{air} (P_i - P_d)}$ $\dot{m}_d = Cd_v L_g h_{max} \sqrt{2\rho_{air} (P_i - P_d)}$ $-Cd_o A_o \sqrt{2\rho_{air} (P_d - P_{atmos})}$ $\dot{m}_s = Cd_o A_o \sqrt{2\rho_{air} (P_{atmos} - P_s)}$
$P_i < P_d$ & $P_i > P_{atmos}$	$\dot{m}_i = 0$ $\dot{m}_d = -Cd_o A_o \sqrt{2\rho_{air} (P_d - P_{atmos})}$ $\dot{m}_s = Cd_o A_o \sqrt{2\rho_{air} (P_{atmos} - P_s)}$
$P_i < P_d$ & $P_i < P_{atmos}$	$\dot{m}_i = Cd_v L_g h_{max} \sqrt{2\rho_{air} (P_s - P_i)}$ $\dot{m}_d = -Cd_o A_o \sqrt{2\rho_{air} (P_d - P_{atmos})}$ $\dot{m}_s = Cd_o A_o \sqrt{2\rho_{air} (P_{atmos} - P_s)}$ $-Cd_v L_g h_{max} \sqrt{2\rho_{air} (P_s - P_i)}$

side is given by an equation with is analogous to Equation 5, where  $V_s$  is the volume of the plenum on the inhalation side:

$$\dot{P}_s = \frac{c_s^2}{V_s} \dot{m}_s \quad (7)$$

As in Phase 4, the force acting on the surface of the water column due to the pressure acting on it depends on the state of

the valves. If the exhalation valve is open and the inhalation valve is closed, Equation 6 applies. If the inhalation valve is open and the exhalation valve is closed, this equation is modified to:

$$F_e = (m_7 + a_\infty) \ddot{U}_7 + \int_0^\infty k_7(t - \tau) \dot{U}_7(\tau) dt + c_{77} \dot{U}_7 + (P_{atmos} - P_s) \times A_{owc} \quad (8)$$

No further variables are required in Phase 6. The mass flow rate equations for this phase are summarised in Table III. Again, the force acting on the water column due to the pressure

TABLE III: Mass flow equations - Phase 6

Case	Mass flows
$P_i > P_d$ & $P_i > P_{atmos}$	$\dot{m}_i = -C d_v L_g h_{max} \sqrt{2\rho_{air} (P_i - P_d)}$ $\dot{m}_d = C d_v L_g h_{max} \sqrt{2\rho_{air} (P_i - P_d)}$ $-C d_o A_o \sqrt{2\rho_{air} (P_d - P_s)}$ $\dot{m}_s = C d_o A_o \sqrt{2\rho_{air} (P_d - P_s)}$
$P_i < P_d$ & $P_i > P_{atmos}$	$\dot{m}_i = 0$ $\dot{m}_d = -C d_o A_o \sqrt{2\rho_{air} (P_d - P_s)}$ $\dot{m}_s = C d_o A_o \sqrt{2\rho_{air} (P_d - P_s)}$
$P_i < P_d$ & $P_i > P_{atmos}$	$\dot{m}_i = C d_v L_g h_{max} \sqrt{2\rho_{air} (P_s - P_i)}$ $\dot{m}_d = -C d_o A_o \sqrt{2\rho_{air} (P_d - P_s)}$ $\dot{m}_s = C d_o A_o \sqrt{2\rho_{air} (P_d - P_s)}$ $-C d_v L_g h_{max} \sqrt{2\rho_{air} (P_s - P_i)}$

on the free surface depends on the state of the valves. If the exhalation valve is open and the inhalation valve is closed, Equation 6 applies. If the inhalation valve is open and the exhalation valve is closed, Equation 8 applies.

The density of air within a chamber is one parameter upon which a mass flow rate depends. This density varies due to the compression of air. As shown in [10], for an adiabatic process, the linearised relationship between air density and pressure is given by:

$$\rho_{air} = \rho_{atmos} \left( 1 + \frac{P}{\gamma \rho_{atmos}} \right) \quad (9)$$

## VI. NUMERICAL MODELLING

Typically, the development of any prototype wave energy converter comprises two complimentary strands: physical testing and numerical modelling. Each strand informs the other, with the goal of developing a reliable model which can limit the need for further potentially expensive and time-consuming physical testing. A number of tools were employed to solve the coupled systems of ODEs used to represent the model OWC mathematically. The equations were rewritten in matrix form as a system of coupled first order ODEs. Each phase of testing is modelled by a different system of coupled equations. By way of example, Equation 10 illustrates the coupled first order system for the OWC when configured with a single orifice

in communication with atmosphere (Phase 2). This system is represented by:

$$\dot{X}(t) = AX(t) + Bu(t) \quad (10)$$

where  $X(1) = U_7$ ,  $X(2) = \dot{U}_7$  and  $X(3) = \Delta P = (P_i - P_{atmos})$ .

Using Equations 1 and 2 and making  $\dot{X}(1)$ ,  $\dot{X}(2)$  and  $\dot{X}(3)$  the subjects yields:

$$\dot{X}(1) = \dot{U}_7 = X(2),$$

$$\dot{X}(2) = \ddot{U}_7 = \frac{F_e}{[m + a_\infty]} - \frac{\int_0^\infty k_7(t - \tau) X(2)(\tau) dt}{[m + a_\infty]} - \frac{c_{77}}{[m + a_\infty]} X(1) - \frac{A_{owc}}{[m + a_\infty]} X(3),$$

and

$$\dot{X}(3) = \dot{\Delta P} = \frac{cs^2}{A_{owc}[h_o - X(1)]} \dot{m}_i + \frac{\gamma(x(3) + P_{atmos})}{[h_o - X(1)]} X(2)$$

The matrices  $A$ ,  $B$  and  $u$  of Equation 10 are now written as:

$$A = \begin{bmatrix} 0 & 1 & 0 \\ -\frac{c_{77}}{[m_7 + a_\infty]} & 0 & -\frac{A_{owc}}{[m_7 + a_\infty]} \\ 0 & \frac{\gamma(x(3) + P_{atmos})}{[h_o - x(1)]} & 0 \end{bmatrix}$$

$$B = \begin{bmatrix} 0 & 0 \\ (F_e - \int_0^\infty k_7(t - \tau) \dot{U}_7(\tau) dt) & 0 \\ 0 & \frac{cs^2}{A_{owc}[h_o - x(1)]} \end{bmatrix}$$

and

$$u = \begin{bmatrix} \frac{1}{[m_7 + a_\infty]} \\ \dot{m}_i \end{bmatrix}$$

This system of ODEs can be expanded to model the remaining test phases. Once populated, the system is solved using Runge-Kutta methods implemented in the programming environment MATLAB. In order to populate the values of these equations, AutoCAD is used to determine the volume – and hence the mass – of the water column, as well as the free surface area of the water column (to which the coefficient of buoyancy is directly related). As the water column mass and the coefficient of buoyancy vary with the height of the water column, AutoCAD was used to determine these values for water column heights varying in increments of 1 mm around the still water level. By fitting quadratic curves, the relationship between the displacement and the mass of the water column, the displacement and the volume of air and the displacement and the area of the water column can be included in the numerical model. These values are recalculated at each time step based on the instantaneous water column displacement. The hydrodynamic parameters, such as the frequency dependent exciting force, added mass and radiated damping, are determined using the boundary problem solver WAMIT V7 [11]. WAMIT is a 3-dimensional solver, whereas the testing described herein took place in a 2-dimensional tank. Thus, the results must be considered caution. Future work will compare

the 3-dimensional numerical results with some techniques to generate 2-dimensional results from WAMIT and also with the results of tank testing. However, the issues described in this section remain valid.

Only the pumping mode, assigned the subscript 7, is considered. The geometry of the mean wetted surface of the model OWC tested here, which is required as an input to WAMIT, is generated using the CAD package, MultiSurf [12]. Figure 7 illustrates this geometry. Note that, for clarity, the free surface of the water column is shown in blue in this figure.

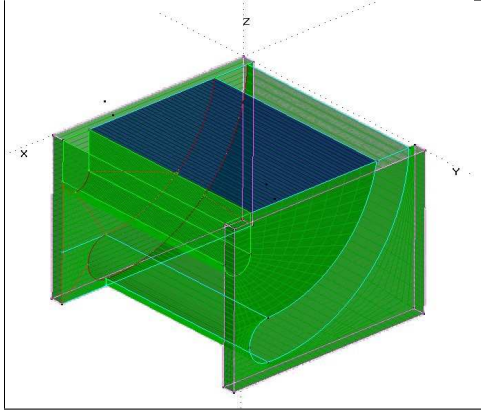


Fig. 7: MultiSurf model of the mean wetted surface of the OWC.

Initially, when solving the coupled system of ODEs described in Equation 10, the impulse response function was constructed from the frequency domain data obtained from WAMIT, and Equation 10 was solved while performing the convolution integral between the kernel,  $k_7$ , and the velocity,  $\dot{U}_7$ , at each time step. However, this is computationally expensive – see, for example, [13] – and the convolution integral was replaced with a state-space representation as described in [14]. This process approximates the convolution integral with a state-space system with zero initial conditions as follows:

$$\begin{aligned} \dot{X}_p(t) &= A_p X_p(t) + B_p u_p(t) \\ y_p(t) &= C_p X_p(t) \approx \int_0^\infty k_7(t - \tau) \dot{U}_7(\tau) dt \end{aligned} \quad (11)$$

The order of the coupled ODEs in Equation 10 increases by the order of the system in Equation 11, and the matrices  $A$  and  $B$  are re-written as:

$$A = \begin{bmatrix} & 0 & & 0 \\ & \vdots & & \vdots \\ A_p & & B_p & \\ 0 & \dots & 0 & 1 \\ -\frac{C_p}{(m_7(t)+a_\infty)} & -\frac{c_{77}(t)}{(m_7(t)+a_\infty)} & 0 & -\frac{A_{owc}}{(m_7(t)+a_\infty)} \\ 0 & \dots & \frac{\gamma(x(7)+P_{atmos})}{(h_o-x(5))} & 0 \end{bmatrix}$$

$$B = \begin{bmatrix} 0 & 0 \\ \vdots & \vdots \\ 0 & 0 \\ Fe & 0 \\ 0 & \frac{cs^2}{A_{owc}[h_o-x(1)]} \end{bmatrix}$$

The vector  $u$  remains unchanged. In order to populate and determine the order of the matrices  $A_p$ ,  $B_p$  and  $C_p$  above, the Marine Systems Simulator (MSS) frequency domain identification tool [15] developed at the Norwegian University of Science and Technology (NTNU), was used. This toolbox requires vectors comprising the frequency dependent radiated damping, added mass and corresponding frequencies, and, optionally the infinite frequency added mass, for the mode of motion in question. The output is a state-space representation of the radiation forces for that mode. However, it was found that when the parameters determined by WAMIT for the pumping mode of the OWC were passed to this tool, the resultant state-space system (irrespective of what order system was generated by the MSS toolbox) was unstable. Thus, the impulse response of the state-space system did not approximate the impulse response function constructed from the frequency dependent radiated damping as found by truncating the integral given by:

$$K(t) = \frac{2}{\pi} \int_0^\infty B(\omega) \cos(\omega t) d\omega \quad (12)$$

This problem would appear to relate to the values calculated by WAMIT for the added mass at higher frequencies and for the infinite frequency added mass. A plot of the dimensionalised added mass versus frequency as calculated by WAMIT can be seen in Figure 8 labelled ‘Unreconstructed’. The dimensionalised infinite frequency added mass returned by WAMIT V7 is given as 356 kg. The added mass curve should be asymptotic to the infinite frequency added mass. However, not only is the curve not asymptotic to the value calculated by WAMIT, this value is also an order of magnitude greater than all other values of added mass determined by WAMIT. Further, the form of the added mass curve is unusual when compared to the equivalent curve for one of the six rigid body modes of regular shapes (see, for example [14]) in so far as, at high frequencies, the values of the added mass for the water column tend towards zero rather than towards the calculated (but anomalous) value for the infinite frequency added mass. While the cause of this issue is unknown at this time, it may relate to how WAMIT solves for the radiation potential, and the tendency for Green’s integral equations to become singular as the thickness of the body (or part of the body) decreases [11]. Similar results were yielded when the process was repeated for the predefined unmodified cylindrical OWC in WAMIT, suggesting the issue does not lie with the geometry of the model. Finally, it is worth noting that the model geometry had previously been analysed using WAMIT V6, and while the added mass versus frequency curve was of similar form, the earlier version of WAMIT calculated an infinite frequency added mass of 46.8 kg, which, while of the same order as the added mass values calculated at non-infinite frequencies, is still greater than all

the non-infinite frequency added mass values determined by WAMIT V6.

However, the frequency dependent added mass and the time

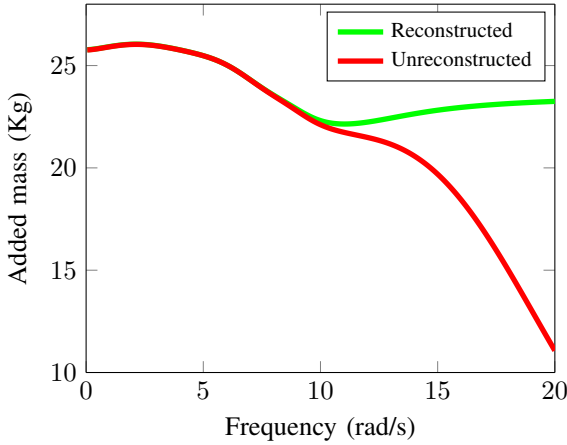


Fig. 8: Dimensionalised frequency dependent added mass from WAMIT V7 and reconstructed from radiated damping for the OWC shown in Figure 7.

dependent impulse response are related through the Kramer-Kronig relation as follows:

$$A(\omega) = A_{\infty} - \frac{1}{\omega} \int_0^{\infty} K(t) \sin(\omega t) dt \quad (13)$$

Thus, it is possible to use the impulse response as constructed from the radiated damping using Equation 12 to calculate the added mass using Equation 13 once the correct value of  $A_{\infty}$  is known. While the radiated damping calculated by WAMIT for the OWC (shown in Figure 9) would appear to be of the correct form, in order to establish confidence in these values, a thin-walled narrow pipe of draft 0.18 m and radius 0.0225 m was modelled in WAMIT as a single dipole patch with a second patch representing the water column surface. The radiated damping of the water column in this pipe was determined in WAMIT, and the results compared to those calculated using the analytical solution given in [16] as:

$$B(\omega) = M\omega \frac{\pi}{2} \left(\frac{b}{a}\right)^2 K a e^{-2Ka} \quad (14)$$

where  $M$  is the mass of the water column,  $a$  is the draft of the pipe,  $b$  is the radius of the pipe and  $K = \frac{\omega^2}{g}$ . The comparison between these results is shown in Figure 10 where the closed form results were obtained from the solution of Equation 14. It can be seen there is good agreement between these two data sets. However, before the frequency dependent added mass values may be reconstructed using Equation 13 with the impulse response function constructed from radiated damping values using Equation 12, it is necessary to determine the appropriate value of  $A_{\infty}$ . It can be seen from Equation 13 that the shape of a curve plotting the frequency dependent added mass determined from this equation against frequency is not dependent on  $A_{\infty}$ . However, the y-intercept of this curve is dependent on  $A_{\infty}$ . The curve labelled 'Reconstructed'

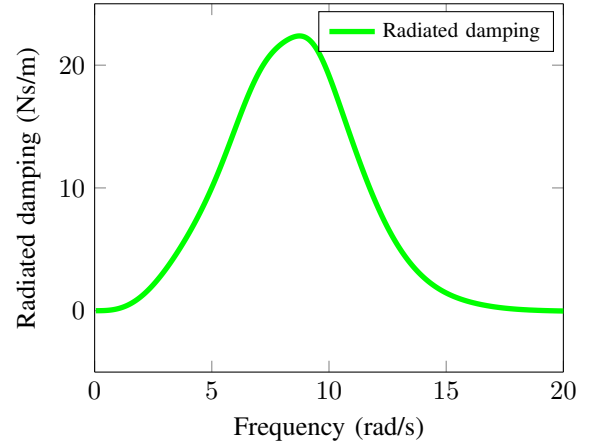


Fig. 9: Radiated damping calculated by WAMIT V7 for the OWC shown in Figure 7.

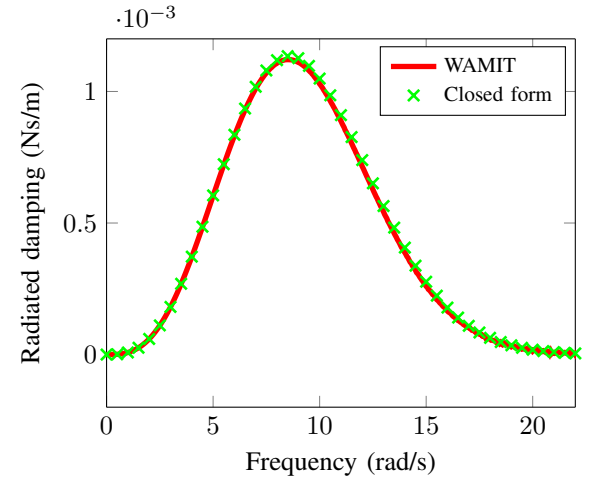


Fig. 10: Comparison of radiated damping calculated from WAMIT V7 and closed form solution for a thin-walled pipe.

in Figure 8 illustrates the frequency dependent added mass determined using Equation 13 with the radiated damping values from WAMIT V7 and  $A_{\infty}$  set equal to 23.55 kg. The effect of varying  $A_{\infty}$  would be to cause the y-intercept of this curve to increase or decrease, and the 'Reconstructed' curve would follow, while retaining the shape shown in Figure 8. The value of  $A_{\infty}$  used was chosen so that the values of the reconstructed added mass would be coincident with the unreconstructed values calculated by WAMIT V7 from 0 to 8 rad/s. Note further that the 'Reconstructed' added mass curve is of similar form to those in the literature for rigid body modes, for example [14]. The reconstructed added mass values found using Equation 13, the infinite frequency added mass value of 23.55 kg and the radiated damping values calculated by WAMIT V7 were used as inputs to the MSS toolbox. The resulting state-space system is stable, and Figure 11 illustrates the comparison between the impulse response for this state-space system and the impulse response determined using

Equation 12. It can be seen that good agreement exists between the two suggesting that the approach used to determine a value for the frequency dependent added mass values and for  $A_\infty$  is valid in this case.

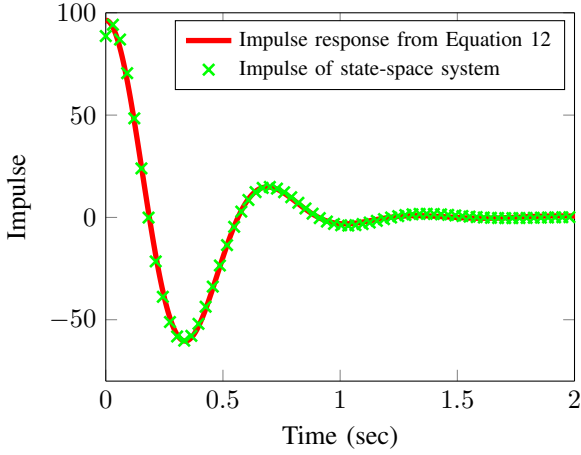


Fig. 11: Comparison of the impulse response of the pumping mode of the OWC as constructed from Equation 12 and the impulse response of the state-space approximation.

Consider now the exciting force. For the two-dimensional case, the Haskind relation between the magnitude exciting force and the radiated damping is given by [17]:

$$|F_e(\omega)| = A\sqrt{\frac{\rho g^2}{\omega} B(\omega)} \quad (15)$$

where  $A$  is the wave amplitude. The relationship between the magnitude of the exciting force and radiated damping for the heave mode of a body in the three-dimensional case is given by:

$$|F_e(\omega)| = A\sqrt{\frac{4\rho g V_g}{K} B(\omega)} \quad (16)$$

where

$$V_g = \frac{g}{2\omega}, K = \frac{\omega^2}{g}$$

Figure 12 illustrates the magnitude of the exciting force for mode 7 of the OWC as calculated by WAMIT V7, and the two- (Equation 15) and three-dimensional (Equation 16) Haskind forces based on the radiated damping calculated in WAMIT V7 for the OWC shown in Figure 7. If it is assumed that the radiated damping is correct, it can be seen that the magnitude of the exciting force calculated by WAMIT appears to be a combination of the two- and three-dimensional Haskind forces. Future work will compare the results shown in this figure with some techniques to generate 2-dimensional results from WAMIT and also results from tank testing.

## VII. SAMPLE RESULTS

Work on calibrating and validating the numerical model based on the results of the narrow tank testing is ongoing. By way of example of the efforts towards producing a validated model, some results from a single test run during Phase 2 of

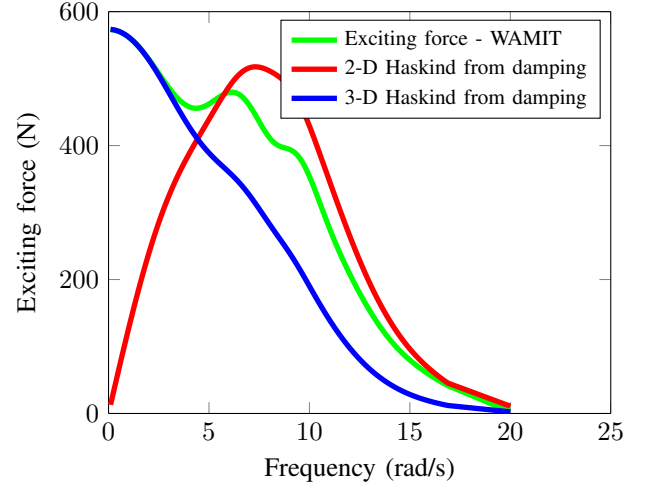


Fig. 12: Exciting force acting on the pumping mode on the water column shown in Figure 7 calculated by WAMIT V7, and showing the 2-D and 3-D Haskind forces calculated from the radiated damping.

the testing are compared to the prediction from the current numerical model. This numerical model uses a value of 23.55 kg for the infinite frequency added mass and a state-space approximation for the convolution integral as determined from the reconstructed added mass values derived as above in Equation 1. A value of 0.6 for the coefficient of discharge is used in Equation 3 as recommended in [8]. Figure 13 illustrates the predicted gauge pressure in the OWC chamber plotted against that obtained during the test for a wave amplitude of 20 mm, with a frequency of 0.4 Hz and an orifice opening diameter of 20 mm, equivalent to a full-scale wave of amplitude 1 m and period 17.7 s. At this frequency, the motion of the water column is dominated by the pumping mode. Figure 14 shows

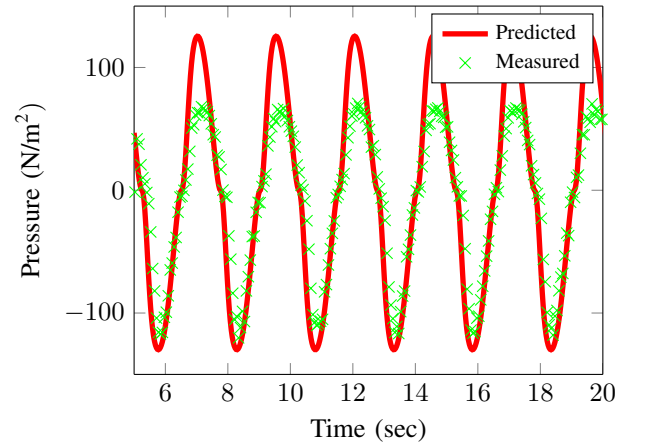


Fig. 13: Gauge pressure in OWC chamber as predicted by numerical model and measured during tank test.

the predicted pumping motion of the water column compared to that observed during the test. It can be seen that good agreement has been obtained for the water column motions

in this instance.

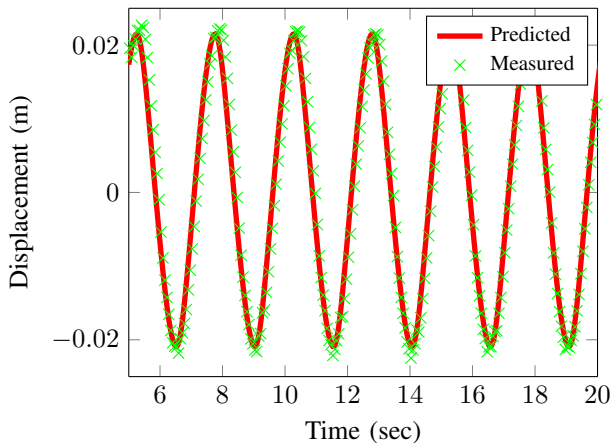


Fig. 14: Water column displacement as predicted by numerical model and measured during tank test.

Good agreement has also been obtained for the inhalation pressures for the specific test conditions listed. However, the exhalation pressures are over-predicted by the numerical model. The gauge pressures in the OWC chamber obtained during the narrow tank testing exhibit asymmetry about zero. This pattern is apparent for all tests during Phase 2, and the asymmetry increases as the amplitude of the water column motion increases. It was considered that this effect may be due to the nature of the iris valve employed, which comprises a number of moving, overlapping segments. However, the effect is also present in the results obtained during Phase 3 of the testing when the iris valve was not employed. As noted in various texts including [10], the processes at work within the chamber are not identical for the inhalation and exhalation stages. As observed in [10], the air mixing process takes place outside the OWC chamber during exhalation, but inside the chamber during inhalation. The results here suggest that the assumption of isentropic conditions may be valid during the inhalation phase, but may not be valid during the exhalation phase. Some success has been had in modelling the exhalation phase as an isothermal process, work which it is hoped will be the subject of future publications.

### VIII. CONCLUSIONS

A programme of narrow tank testing on a single, fixed OWC has been completed. Data has been gathered which may be used to characterise various control components and explore non-linear effects within the system. This work continues and will serve to inform future numerical models of a floating, MOWC device. A process to overcome an issue with the values calculated by WAMIT for the frequency dependent added mass and infinite frequency added mass for use with the frequency domain identification toolbox produced by NTNU has been presented. Theory to model the behaviour of an OWC with an orifice in which the convolution term in the Cummins Equation is replaced by a state-space system has been introduced. For a presented instance, the numerical

model successfully predicted the motions of the water column. However, while the numerical model predicted the gauge pressure within the chamber during the inhalation phase of the motion of the water column with a degree of accuracy, it was less accurate during the exhalation phase for this case. This is possibly due to the assumption of isentropic conditions, and the numerical model will be refined in further work to investigate this phenomenon.

### ACKNOWLEDGEMENTS

The authors wish to acknowledge the Carpentry and Joinery Department of DkIT for their assistance in the construction of the marine plywood model used during the narrow tank testing described herein. The first author further wishes to acknowledge the management of WEI Ltd. for providing access to materials and intellectual property within the framework of research being undertaken pursuant to his PhD, and the Irish Research Council for providing funding for this research.

### REFERENCES

- [1] T. Kelly, T. Dooley, J. Campbell, and J. V. Ringwood, "Comparison of the experimental and numerical results of modelling a 32-oscillating water column (OWC), V-shaped floating wave energy converter," *Energies*, vol. 6, no. 8, pp. 4045–4077, 2013. [Online]. Available: <http://www.mdpi.com/1996-1073/6/8/4045>
- [2] —, "Modelling and results for an array of 32 oscillating water columns." *Tenth European Wave and Tidal Energy Conference*, 2013.
- [3] A. Iturrioz, R. Guanche, M. Alves, C. Vidal, and I. Losada, "Time-domain modeling of a fixed detached oscillating water column towards a floating multi-chamber device," *Ocean Engineering*, vol. 76, pp. 65–74, 2014.
- [4] Wave Energy Ireland Ltd, "Analysis of wave flume testing of WEI models at the HMRC, Cork," CREDIT DkIT, Tech. Rep., November 2010.
- [5] D. P. Georgiou, K. F. Milidonis, and E. N. Georgiou, "Sensitivity analysis for the engaged turbine concept in oscillating water column plants," *ISRN Renewable Energy*, vol. 2012, no. 1, pp. 1–8, 2012.
- [6] W. Cummins, *The Impulse Response Function and Ship Motions*, ser. Technical Report 1661. Department of the Navy, David Taylor Model Basin, 1962.
- [7] A. Hazem, S. Noor, S. Bashi, and H. Marahban, "Mathematical and intelligent modeling of electropneumatic servo actuator systems," *Aust. J. Basic Appl. Sci.*, vol. 3, no. 4, pp. 3663–3671, 2009.
- [8] ISO, "Measurement of fluid flow by means of pressure differential devices inserted in circular cross-section conduits running full — Part 2: Orifice plates," International Organization for Standardization, Geneva, Switzerland, ISO 5167-2:2003, 2003.
- [9] R. A. Habing, "Flow and plate motions in compressor valves," Ph.D. dissertation, Twente University Holland, 2005.
- [10] W. Sheng, R. Alcorn, and T. Lewis, "On thermodynamics in the primary power conversion of oscillating water column wave energy converters," *Journal of Renewable and Sustainable Energy*, vol. 5, no. 023105, 2013.
- [11] WAMIT Inc., *WAMIT User Manual Version 7.0*. MA USA: WAMIT Inc, 2012, vol. 1.
- [12] AeroHydro Inc., *MultiSurf 8.0*, Maine USA, 2011.
- [13] R. Taghipour, T. Perez, and T. Moan, "Hybrid frequency-time domain models for dynamic response analysis of marine structures," *Ocean Engineering*, vol. 35, no. 1, pp. 685–705, 2008.
- [14] Z. Yu and J. Faldes, "State-space modelling of a vertical cylinder in heave," *Applied Ocean Research*, vol. 17, no. 5, pp. 265–275, 1995.
- [15] T. Perez and T. I. Fossen, "A Matlab Toolbox for Parametric Identification of Radiation-Force Models of Ships and Offshore Structures," *Modeling, Identification and Control*, vol. 30, no. 1, pp. 1–15, 2009.
- [16] D. Evans, "The oscillating water column wave-energy device," *J. Inst. Maths. Applied*, vol. 22, pp. 423–433, 1978.
- [17] N. Newman, "The exciting forces on fixed bodies in waves," *Journal of Ship Research*, vol. 6, no. 3, pp. 10–17, 1962.